Mechanism of Carbon Filament Growth on Metal Catalysts

R. T. YANG AND J. P. CHEN

Department of Chemical Engineering, State University of New York, Buffalo, New York

Carbon filaments formed on Ni, Co, and α-Fe particles by reaction with methane were studied. The filaments contained faceted single-crystal metal particles located at the growing tips. The crystallographic orientations of the gas/metal and graphite/metal interfaces were identified by TEM/selected area diffraction. Furthermore, extended Hückel molecular orbital calculations indicated that the (111) and (311) faces of Ni provide stronger epitaxial fits with graphite than the (100) and (110) faces and that the order is reversed for their activities for CO decomposition. The results are in agreement with the limited amount of literature data on phase segregation and surface reconstruction for carbon/metal solid solutions. On the basis of these and literature results, a better understanding of the carbon dissolution/diffusion/precipitation mechanism for filament growth is obtained. Also, a temperature-driven carbon diffusion mechanism without resorting to the exothermality of the surface reaction is proposed. © 1989 Academic Press, Inc.

INTRODUCTION

Carbon deposition on metal and catalyst surfaces when heated in the presence of carbon-containing gases is an important problem. The carbon formed has a wide variety of physical and chemical structures, ranging from graphitic carbon to amorphous coke (hydrocarbon). The vast literature on the subject has been reviewed in a number of papers (*1–5*). Of particular interest is the formation of filamentous carbon.

Filamentous carbon is formed on small metal particles, e.g., on supported catalysts or polycrystalline metals having small grain sizes. The sizes of the particles for the formation of carbon filaments are typically less than 0.5 μm. A common characteristic of all carbon filaments is that the metal particle is found at the growing tip of the filament. The metal particles are usually faceted. Studies on the microstructure indicate that the filaments are graphitic with a fishbone structure and that the graphitic layers are stacked parallel to the metal surfaces (*6–9*). Figure 1 illustrates the present understanding of the growth process and the graphitic structure on an idealized cone-shaped particle. Evidence has been shown both for (*10, 11*) and against (*5*) the existence of metal carbides as necessary intermediate for filament growth. Tibbetts *et al.* (*12*) recently showed experimental results that filaments of varying desired lengths and diameters can be grown by properly changing the hydrocarbon/hydrogen ratio, and their calculations based on an adsorption/diffusion model can explain the experimental growth rates. Alstrup (*13*) hypothesized that an "unstable carbide" which causes reconstruction of the metal particle is formed, followed by its decomposition into a "surface carbide" at the gas/metal interface. However, experimental evidence (e.g., by hot-stage XRD) remains to be seen for this hypothesis.

Although much information has been revealed in the vast literature on the subject, little attention has been paid to the growth process at the metal/graphite interfaces. The work of Blakely and co-workers on phase segregation, i.e., the precipitation of carbon from solid solution of carbon in metal as temperature is lowered, has shown some important results for the process (*14–16*). Consequently, our effort was focused on the phase segregation process during the growth of filamentous carbon. The specific
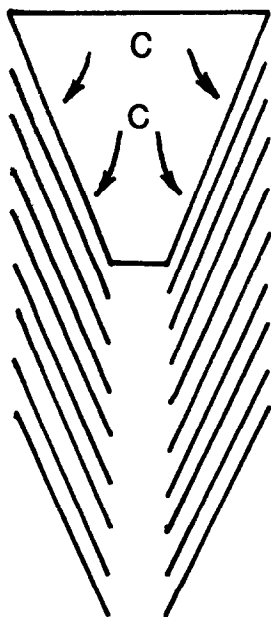
FIG. 1. Schematic for filament growth on an idealized cone-shaped metal particle. The following steps are involved: decompositions of hydrocarbon on the top surface, diffusion of carbon in metal, and precipitation of graphite forming a filament. Note that the (002) planes of the graphite are parallel to the metal/graphite interfaces.

objective of this work was to determine the crystallographic faces of the metal particles upon which graphite layers are formed. The selected area electron diffraction (SAD) technique has been used by Audier *et al.* (*7, 8*) to determine the gas/metal interfaces. This technique was used in this work to characterize the graphite/metal interfaces for Ni, Co, and α-Fe (Ni and Co have fcc structures, whereas α-Fe has a bcc structure).

In addition to the SAD results on the graphite/metal interfaces, the extended Hückel molecular orbital (EHMO) calculations were made to provide semiquantitative information on (i) the epitaxial relationship between graphite and different crystallographic Ni faces and (ii) the relative catalytic activities of different Ni faces for decomposition. This information was obtained from the EHMO results on binding energies, reduced overlap populations,

and charge distributions. The latter information also helped resolve the conflicting results on relative activities reported in the literature.

EXPERIMENTAL: TEM/SAD

Carbon filaments were grown on fine particles of Ni, Co, and α-Fe supported on alumina, by exposure to CH_4 at 1 atm and 700°C for 2 h. The Ni/Al_2O_3 catalyst was supplied by United Catalyst, Inc., designated G-56, which had 17% metal loading. The Co and Fe catalysts were prepared by impregnation of alumina to a final metal loading of approximately 20%. The steps for impregnation were impregnation of aqueous solution of metal nitrate, calcination at 500°C for 8 h, and finally reduction by H_2 at 500°C for 16 h. TEM examinations gave the following sizes for the supported metal particles: Ni, 800–1000 Å, Co, 600–1000 Å, and α-Fe, 800–1200 Å.

The catalyst was heated in a quartz reactor to 700°C slowly (first held at 600°C overnight, then raised to 700°C for reaction) in N_2. The N_2 was O_2-free grade from Linde Division ($<\frac{1}{2}$ ppm O_2), which was further purified by passing through copper turnings at 550°C. Methane (CP grade from Linde Division, 99.0% purity) was introduced to the reactor for 2 h at 700°C. The "coked" sample was cooled to room temperature at approximately 25°C/min and was ready for preparation for TEM/SAD examination. Carbon filaments in the catalyst were freed by dispersing in distilled water in an ultrasonic bath. Using a syringe, a small amount of the aqueous suspension was deposited on a Formvar film supported on a copper grid. The sample was subsequently dried and examined in a TEM (JEOL 100 U). The image rotation angles between TEM and SAD were calibrated by using a hexagonal MoO_3 crystal.

METHOD OF EHMO CALCULATION

The calculations were based on a program originally written by Hoffman (*17*), and the version modified by Bartmess and

Thomas (*18*) was used. The computations were performed on a VAX 8700 computer.

The principles and applications of EHMO in catalysis have been described in several reviews (*19, 20*). Due to the approximations made in EHMO, such as the neglect of core electrons and the use of an approximate energy calculation procedure, this method is not as accurate as CNDO. However, the parametrization of CNDO presents a considerably more difficult problem, and parametrization is now available only for second-row elements (up to F) although estimation techniques for parametrization are available (*21*). The ab initio method is the most rigorous and predictive. It suffers, however, from the requirement of a large amount of computer time. The amount of computation increases sharply with the size of the system and/or inclusion of heavy atoms. Consequently, this method is yet to be used in catalysis. The EHMO, due to its simplicity, is used to provide valuable semiquantitative information for complex systems on catalysis (*22, 23*) and metal clusters (*24, 25*).

EHMO is a semiempirical MO scheme in which the diagonal elements of the Hamiltonian matrix (H_{ii}) in the Slater orbital are taken as the valence state ionization energy (VSIE) (or the negative ionization potential). The off-diagonal elements are taken to be proportional to the average of the two relevant atomic ionization potentials (H_{ii} and H_{jj}) and the overlap integral (S_{ij}), i.e.,

$$H_{ij} = \tfrac{1}{2}KS_{ij}(H_{ii} + H_{jj}),$$

where K is an empirical constant usually taken as 1.75. In this work, the binding energy between graphite and metal was calculated as the difference between the bonded atoms (adatoms plus metal) and the isolated graphite and metal. The overlap populations between two atoms were calculated by the Mulliken procedure (*26*). The input parameters for computation were the atomic parameter, orbital exponents, and charge iteration parameters, shown in Table 1. All EHMO calculations were performed in the manner of charge iteration according to

$$H_{ii} = -\text{VSIE}(Q) = AQ^2 + BQ + C$$

until reaching convergence, where VSIE was for orbital i when the total charge of the atom was Q.

Nickel was chosen as the representative transition metal with fcc structure for all EHMO calculations because it was the metal on which the most extensive information was available. This information included other EHMO calculations, filament growth, catalytic activities, and chemisorption on different faces of Ni. Furthermore, four important faces were chosen for calculations on both epitaxy and activity: (311), (111), (110), and (100). The choice of the sizes of the surface metal cluster and the overlayer is usually an arbitrary one. Robertson and Wilmsen (*27*) showed that, in EHMO calculations of CO on Ni, the chemisorption energy was not significantly influenced by increasing the surface from 8 Ni atoms to 15 atoms. Likewise, calculations with two Ni layers showed that the binding energies were somewhat greater than those with a single layer but the energy minima and other important characteristics were the same. Therefore, 9 Ni atoms were chosen for all four faces in this work. The structures and lattice distances of the four faces are shown in Fig. 2. For Ni(100),
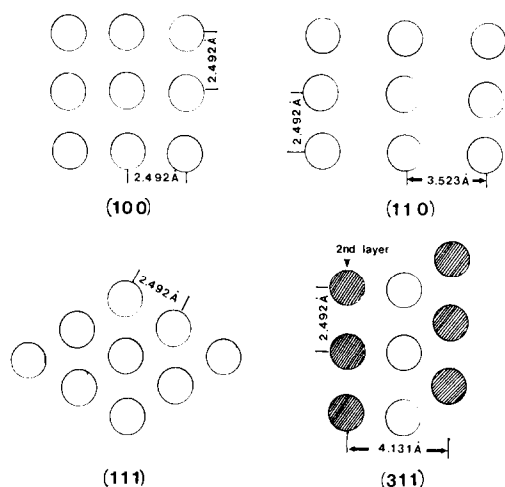
TABLE 1

Parameters Used for EHMO Calculations

Atom	Orbital	Orbital exponent	Coul.	A	B	C	c
Carbon	2s	1.625	−21.4	0.0	11.9	20.4	
	2p	1.625	−11.4	0.0	11.9	10.6	
Oxygen	2s	2.275	−32.3	0.0	15.2	33.0	
	2p	2.275	−14.8	0.0	15.2	16.4	
Nickel	4s	1.825		0.911	8.561	7.54	
	4p	1.125		0.986	6.552	3.89	
	3d	5.75		1.76	13.56	10.9	0.3883
		2.0					0.629

Note. Coul., *A*, *B*, and *C* are in electron volts. Coul. serves as the initial guess for H_{ii}. *A*, *B*, and *C* are constants for calculating VSIE in the procedure of charge iteration, and *c* is the coefficient of *d* orbital exponent.

FIG. 2. Structures and lattice distances of four Ni faces used in EHMO calculations.

RESULTS AND DISCUSSION

Transmission Electron Microscopy/Selected Area Diffraction

Audier et al. have studied the graphite deposition on a number of fcc FeCo and FeNi alloys and bcc FeCo alloys using the TEM/SAD technique (7, 8). The idealized cone-shaped particle (Fig. 1) was chosen for careful examination in their studies. The most important result from their studies is that the bare gas/metal interface (where no graphite is deposited) is (100) for the FeCo allows of bcc structures and is (111) for the FeCo and FeNi alloys of fcc structures. Apparently no attempt was made for the identification of the metal/graphite interfaces.

Over 30 metal/graphite filament composites were studied in this work. These composites contained metal particles in the size range (500–1000 Å) suitable for SAD. Some general observations are first given as follows. SAD spot patterns were obtained for all particles indicating that they were single crystals. Only a few of the metal particles had the idealized cone shape as shown in Fig. 1. They were, however, all faceted

(110), and (111) faces, all 9 atoms are on the same plane, whereas for Ni(311), two layers are shown with a d-spacing of 1.06 Å between the two layers, because the interactions with the adatoms from the 6 second-layer atoms are stronger than those from the more distant first-layer atoms. For graphite/metal epitaxy studies, a graphite layer consisting of 12 carbon atoms was used (Fig. 3). For the catalytic activities of different Ni faces, the decomposition of CO was studied rather than CH_4 because more information was available for CO/Ni for the EHMO calculation, and the same relative activities applied to both CO and CH_4 as will be discussed. For the relative catalytic activity study, each ensemble consisted of 9 Ni atoms and 3 CO arranged in a manner so that a fair comparison could be made on the relative activation of CO. Because the EHMO method is not useful for determining bond lengths, we have chosen a Ni–C bond length of 1.838 Å (28) as the shortest possible in all four ensembles. The ensembles used to calculate CO decomposition activities are shown in Fig. 4. Experimental evidence for the linear configuration of CO on Ni (as used in Fig. 4) has been shown and discussed in the literature (27, 29).
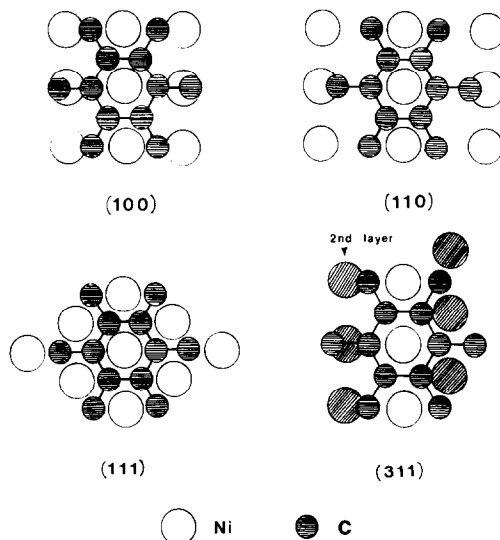

FIG. 3. Graphite/Ni ensembles used for EHMO calculations. The shortest C–Ni bond distance in all ensembles is 1.838 Å, and the C–C bond length is 1.415 Å.
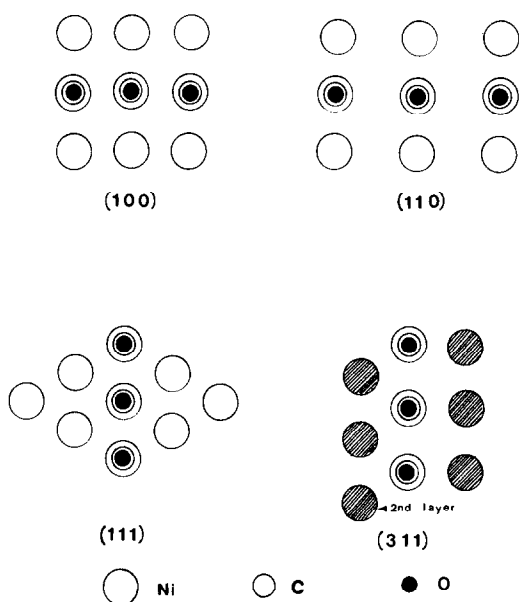
(100) (110)

(111) (311)

○ Ni   ○ C   ● O

FIG. 4. CO/Ni ensembles used for EHMO calculations. Each ensemble contains three linear CO normal to the Ni surface with C closest to Ni where the C–Ni distance is 1.838 Å, and the C–C bond length is 1.415 Å.

with irregular shapes. Representative results are shown next.

Figures 5a and 5b show the SAD patterns (of Ni) superimposed on the bright-field TEM images for the Ni/filament composites. The SAD indexing procedure described by Andrews et al. (30) was followed. The Miller indices calculated according to this procedure are labeled on all SAD patterns. The indices of a given plane on the faceted crystal can be found from the fact that the line connecting a SAD spot with the SAD center is normal to that plane. The images shown here and on all subsequent figures were taken with the electron beam normal to the filament axis (or 0° tilt angle). The results show the possibility of the existence of (002) plane at the gas/metal interfaces, and (111), (311), and (220) planes at the graphite/metal interfaces. Further identification of these interfacial planes would require a goniometer tilt stage in the TEM. To identify the (111)

face, for example, SAD patterns at different tilt angles around the (111) axis are needed. The presence of the (111) reflection in all patterns would further confirm its existence. Figure 6 shows the result for another fcc metal, Co. The result shows that the (111) face is a possible metal/graphite interface and that (220) and (002) faces are possible gas/metal interfaces. The result for the bcc structured α-Fe/filament is shown in Fig. 7. The orientations of the metal/ graphite interfaces could not be matched with the diffractions by all major planes with low Miller indices. However, the following faces possibly existed at the gas/ metal interfaces: (100), (110), and (121). Figure 7 also showed that the filament was hollow. However, hollow filaments were observed only in conjunction with a drawn-out shaped tail in the metal particle, as shown typically in Figure 8. All metal particles shown in Figs. 5–7 were encapsulated by a layer of carbon, due to the long "coking" time. The encapsulation does not, however, interfere with the SAD results and their interpretations. As will be discussed later, encapsulation terminates the filament growth process.

EHMO: Graphite/Metal Epitaxy

On the basis of Mulliken population analysis, Siegbahn and co-workers (31) recently defined covalency and ionicity in chemical bonds to discuss their calculation results. Ionicity is related simply to the total charge whereas covalency is proportional to the reduced overlap population (31). Since the difference in the electron affinities of Ni and C is only 0.7, the chemical bond between Ni and C is mainly (88%) covalent. Therefore, the reduced overlap populations are used for comparing the relative bond strengths between carbon and different Ni faces.

EHMO calculations were performed for four Ni faces, each consisting of 9 atoms and 12 graphite adatoms (Fig. 3). The bond strengths are indicated by the reduced overlap populations, shown in Table 2.
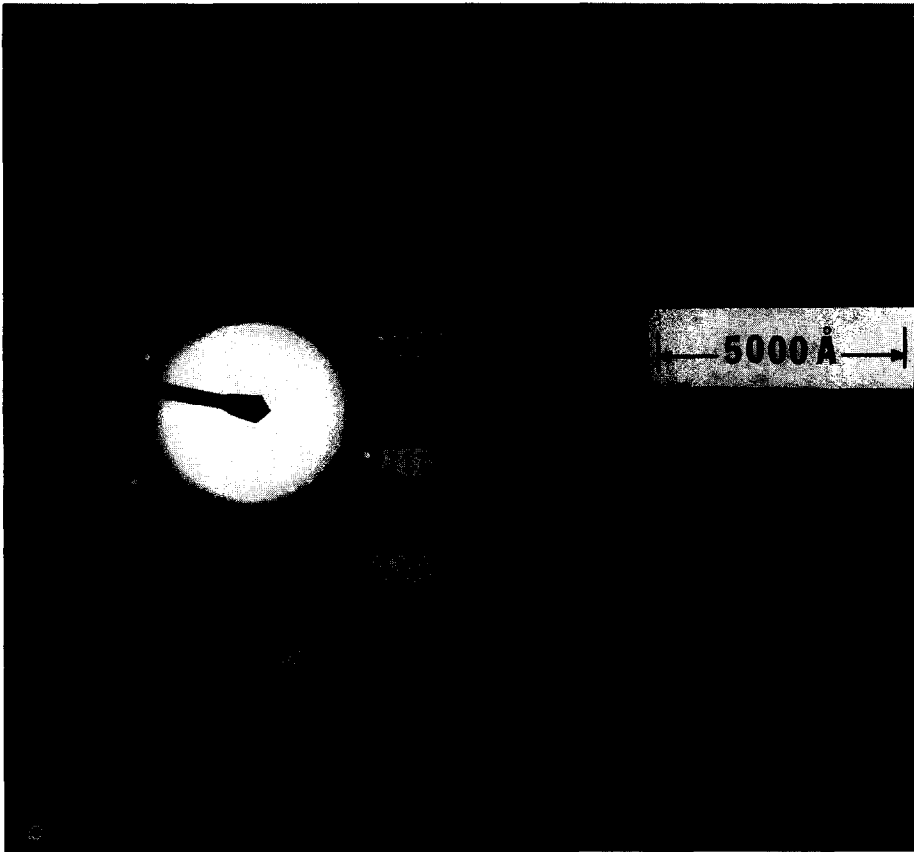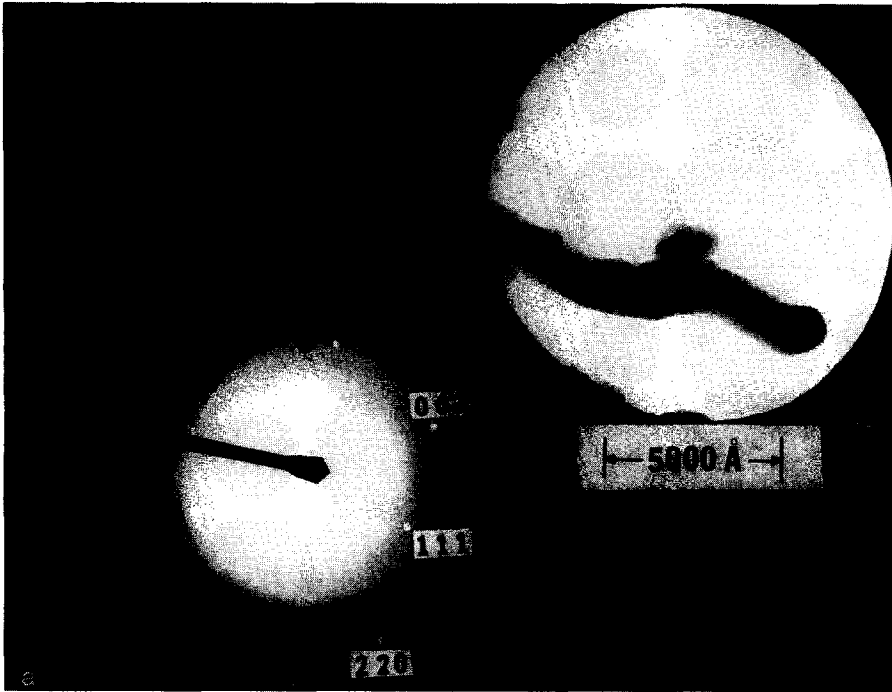
FIG. 5. (a and b) SAD pattern of nickel particle superimposed on the bright-field TEM image of Ni/filament.
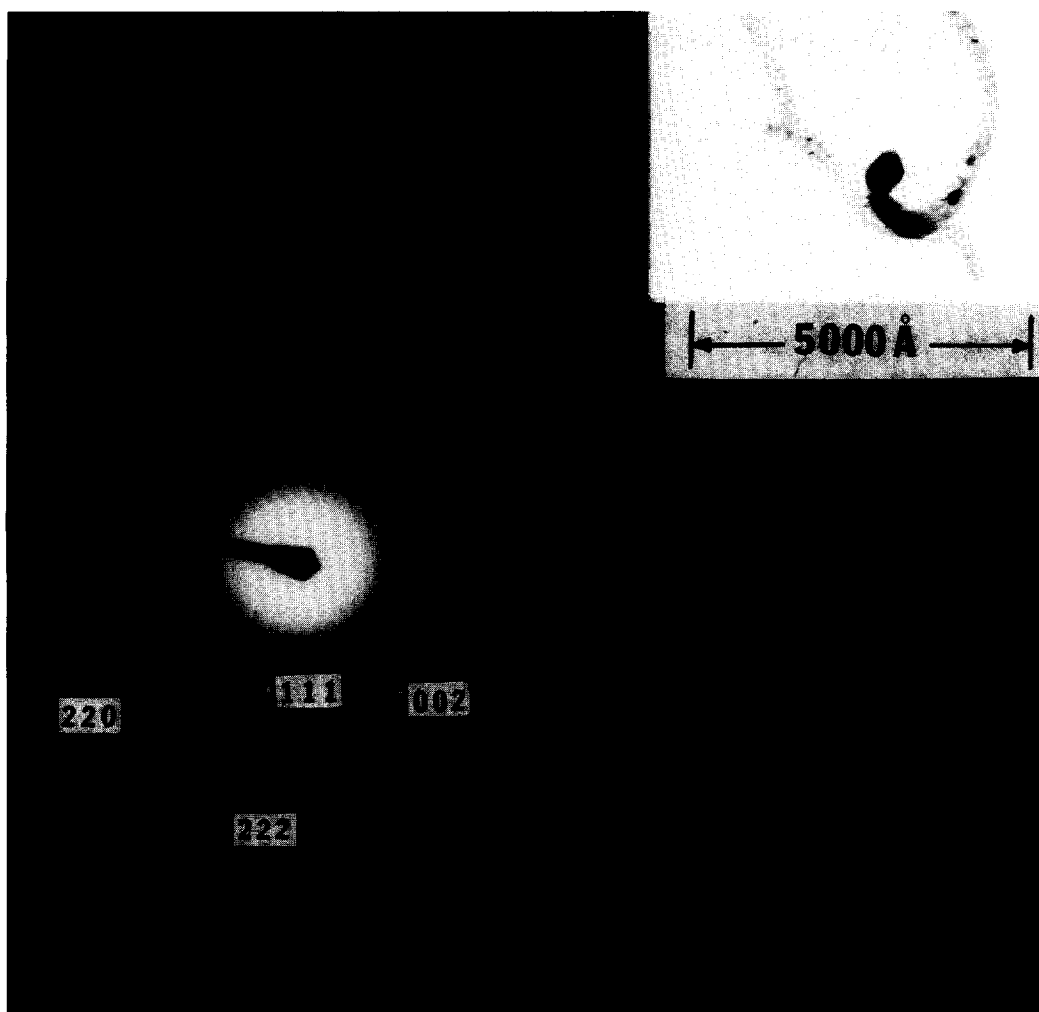
FIG. 6. SAD pattern of Co particle superimposed on the bright-field TEM image of Co/filament.

These values are the sums of all Ni–C pair reduced overlap populations, summed over the whole ensemble. The strongest overlap

TABLE 2

EHMO Results for Total Reduced Overlap Populations (OP) and Binding Energies (BE) between Graphite (12 Atoms) and Ni Faces (9 Atoms)

Ni face	(111)	(311)	(100)	(110)
OP	3.24	1.70	1.81	1.81
BE (eV)	−92.51	−65.09	−52.49	−49.24

is between graphite and Ni(111), giving a value of 3.24 whereas the values for the other three faces are between 1.70 and 1.81. This result indicates that Ni(111) provides the strongest binding to graphite and hence graphite/Ni(111) is the most stable system.

Since the reduced overlap populations of graphite and Ni(311), (110), and (100) faces are nearly the same, further calculations on binding energies and electron transfers are needed to gain an insight into the differences in interactions. the EHMO binding energy results are also summarized in Table 2. The binding energy is taken as the net
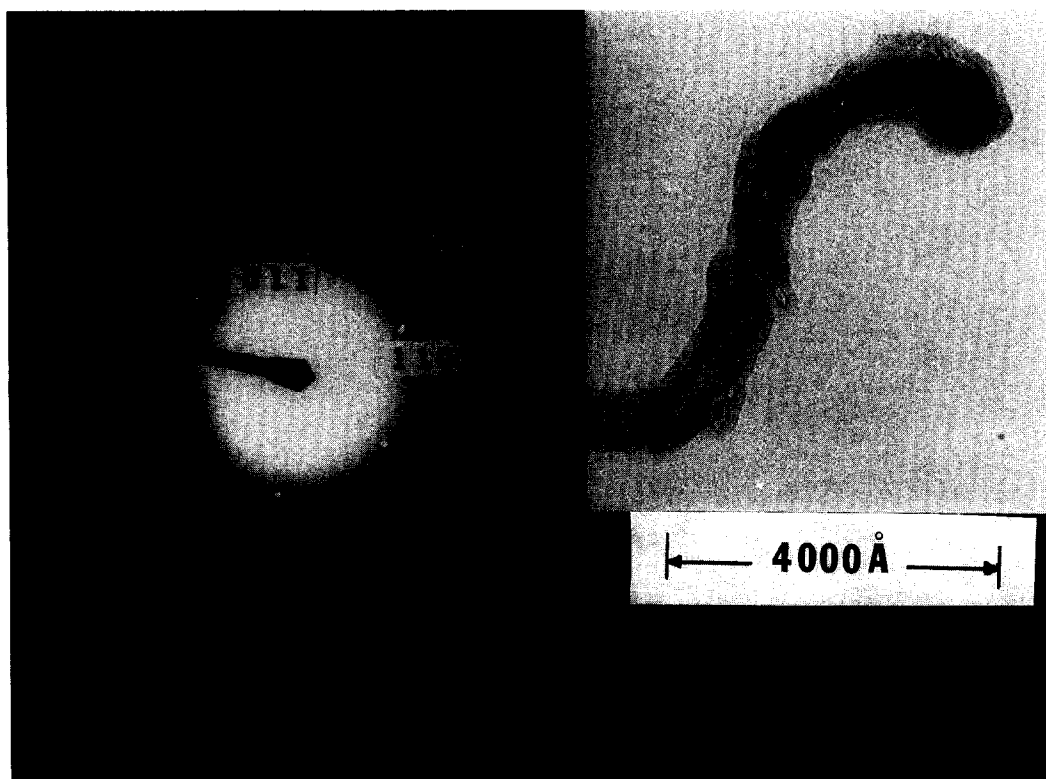
FIG. 7. SAD pattern of α-Fe particle superimposed on the bright-field TEM image of α-Fe/filament.

difference between the total energy of the Ni/C ensemble and the energies of isolated Ni and graphite layers. As discussed in other applications of EHMO, significant differences exist between the calculated and the experimental values (20). The relative values are, however, meaningful. The

TABLE 3

Frontier Orbital Energy Levels and Charge Distribution of Nickel in the 9Ni/12C Ni/Graphite Ensembles

Ni face	(111)	(311)	(100)	(110)	Graphite (0001)
-HOMO, eV	9.953	9.988	9.961	10.244	10.476
-LUMO, eV	9.939	9.963	9.780	9.399	9.423
ΔE_1, eV[a]	0.530	0.565	0.537	0.821	
ΔE_2, eV[a]	0.537	0.513	0.696	1.077	
$\sum_{i=1}^{9} Q_{(Ni)i}$	1.060	0.797	0.424	0.426	

[a] $\Delta E_1 = [E_{(Ni)HOMO} - E_{(C)LUMBO}]$; $\Delta E_2 = [E_{(C)HOMO} - E_{(Ni)LUMO}]$. The summation Q is the net Ni atomic charges of the nine atoms.

binding energy results (Table 2) indicate that the Ni(111) face is most favorable for graphite binding, followed in the order

$$(111) > (311) > (100) > (110).$$

This order agrees in general with the experimental orders for graphite formation on Ni (32, 33). The results of LaCava et al. (33) are (111) > (100) > (110) > (311), and the results of Kehrer and Leidheizer (32) are (111) > (110) > (100).

The results on frontier orbital energy levels of different Ni faces and charge distributions between Ni and C are given in Table 3. The results on net charge (ΣQ) clearly show that Ni(111) donates the most electrons to graphite, with a net charge as high as 1.06. Ni(311) is the next, with 0.80, followed by Ni(100) and Ni(110) with approximately 0.42. The results on electron transfer and those of binding energy are consistent. The frontier energy levels may
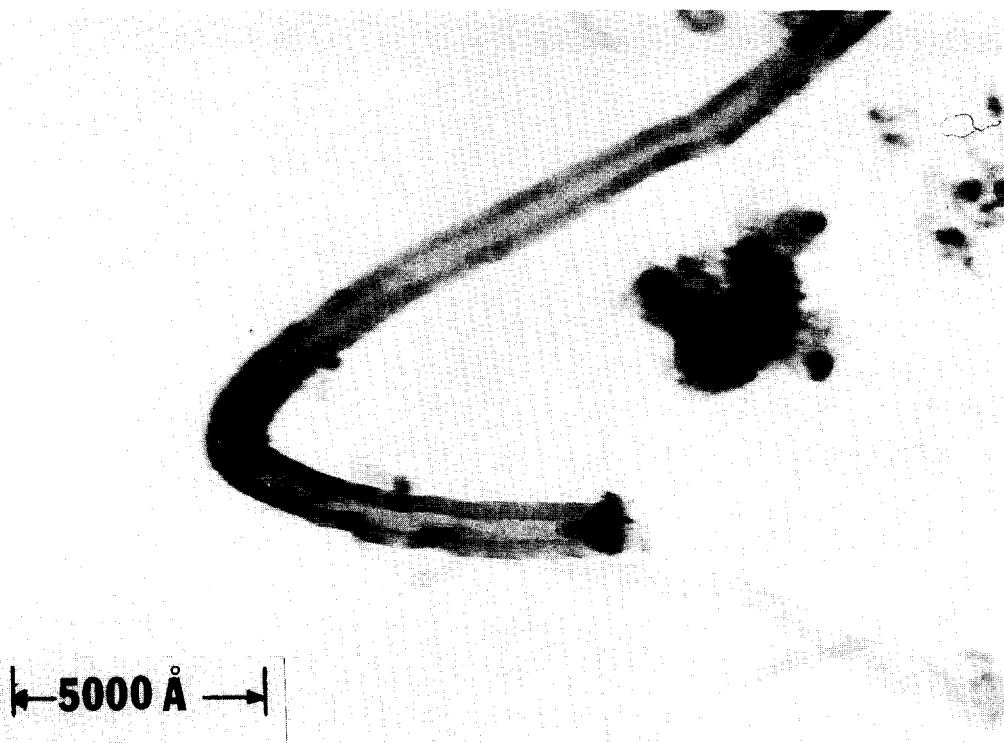
FIG. 8. TEM micrograph of a hollow filament grown on α-Fe/Al$_2$O$_3$ with 1 atm CH$_4$ at 700°C for 2 h.

be used to gain insight into the electron transfer mechanism. Data on highest occupied molecular orbital (HOMO) and lowest unoccupied molecular orbital (LUMO) are also given in Table 3. ΔE's indicate the relative ease of electron transfer from HOMO to LUMO. The interactions between the HOMO of Ni and the LUMO of C are clearly most important in the overall electron transfer. For Ni(110), ΔE_2 is substantially greater than ΔE_1, indicating a lack of ease for electron transfer from Ni to C, whereas the situation is different for Ni(111) and Ni(311).

EHMO: CO/Ni Reactivity

EHMO calculations have also been performed on the same four Ni faces in order to gain an understanding of the relative catalytic activities of these faces in decomposition of hydrocarbons. Literature data have shown that CH$_4$ and CO have the same relative reactivities on different Ni faces. CO has been chosen for this work because of its structural simplicity.

The EHMO results are shown in Table 4. The C═O bond strength is weakened on all four Ni faces, as seen in a comparison of the reduced overlap populations between carbon and oxygen for the adsorbed and

TABLE 4

Overlap Populations and Net Charges on Different Ni Faces

CO/Ni face	Overlap population of C–O	Overlap population of Ni–C	Avg. net charge of CO
(110)	1.338	0.691	−0.20
(100)	1.369	0.707	−0.13
(111)	1.387	0.657	−0.11
(311)	1.404	0.667	−0.08
Free CO	1.449		

free CO. Thus, activation of CO occurs on all four faces. The degree of activation follows the order

$$Ni(110) > (100) > (111) > (311).$$

The same order is also followed for the net charges of CO, also given in Table 4. A higher net charge (electron transfer from Ni to CO) results in a higher activation of CO. The charge transfer is through a σ–π coordinative adsorption mechanism (29) as described as follows. The lone pair electrons of carbon first interact with the empty d-orbital of Ni. This is followed by the interaction between the occupied d-orbital of Ni and the π^* antibonding orbital of CO. Thus, the activation of CO depends on the net electron transfer to the π^* antibonding orbital of CO. The relative activities of the four Ni faces for CO dissociation are clearly indicated by the aforementioned order for CO activation.

The relative activities of three Ni faces for decomposition of CH_4 have been studied at 10^{-2} Torr and temperatures up to 345°C (34). The activity of Ni(110) is higher than that of Ni(100), and Ni(111) does not display activity under these conditions. One of the two types of carbon formed on the surface readily diffuses into the bulk. The relative activities of Ni(111) and Ni(110) have also been studied for acetylene decomposition (0.5 Torr, 1000°C) (35). Again, only Ni(110) is active and no activity is shown by Ni(111). In both of these studies on relative activities (34, 35) thin single-crystal plates were used, with the desired crystal face being the predominant face exposed to the gas phase. Kehrer and Leidheiser (32), on the other hand, studied carbon deposition from CO on a single-crystal sphere, with all crystal faces exposed. They observed the most carbon deposition on the Ni(111) region on the sphere and little on (110) and (100) regions. The activity of carbon far exceeded unity in all studies. The results of this study were likely on the relative epitaxies, not on the relative activities: CO decomposed on the
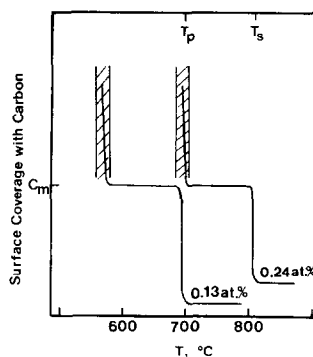

Fig. 9. Equilibria between surface carbon on Ni(111) and bulk C/Ni solid solutions (doped at two different levels). C_m, monolayer carbon; T_p, precipitation temperature; T_s, segregation temperature. Shaded areas are for multilayer graphite precipitation which causes the Ni substratum face to reconstruct for epitaxy with graphite (0001) face.

more active faces into carbon, followed by diffusion through the bulk or on the surface to the (111) region where graphite was formed.

Phase Segregation and Surface Reconstruction

The precipitation of carbon from C/Ni solid solution has been studied extensively by Blakely and co-workers (14, 15), and their results are important in our understanding of the filament growth process. The results relevant to this study are depicted in Fig. 9. A nickel doped with 0.237at.% carbon, i.e., the saturated concentration at 700°C, will be used for discussion. As the sample is cooled to approximately 810°C, a sharp phase transition occurs resulting in a condensed carbon phase on the Ni(111) face. The density of the surface carbon is approximately monolayer. The structure of this "monolayer" is, however, not identical to that of graphite based on LEED results (14). This sharp monolayer carbon transition also occurs on (110), (311), and the (111) vicinal faces of Ni, but a smooth transition was obtained for (100) face (14, 15). The monolayer phase is stable over a temperature span of approximately 110°C upon further cooling,

until the carbon saturation temperature is reached. At the saturation temperature, multilayer single-crystal graphite precipitates and, more importantly, the substratum Ni surfaces reconstruct to mainly (111) and (311) faces to provide epitaxial fits with the (0001) graphite face. Such surface reconstruction seems to be related to that taking place on clean or carbon covered surfaces (36).

Relating the results of Blakely et al. and our results on TEM/SAD and EHMO calculations, the faces for phase segregation and the reconstructed faces identified by Blakely et al. coincide with the graphite/metal interfaces. The most active faces (i.e., 100 and 110) are the gas/metal interfaces. Carbon formed on these faces diffuses into the bulk (34) and precipitates on the graphite/metal interfaces. The agreement of these results provides good evidence that the growth of filaments proceeds by the sequence of carbon dissolution/diffusion/precipitation. Surface reconstruction occurs upon graphite precipitation. Possible epitaxial relationship for (0001) graphite and Ni(111) and Ni(311) are shown in Fig. 3.

As mentioned, the metal particles were faceted upon filament growth. It seems likely that the faceting was caused by the surface reconstruction upon graphite precipitation.

Much has been published on the catalytic activities of different faces of metals and for CO and CH_4 decomposition. Large pieces of single crystals (mm sizes) were used. However, comparison between the large single-crystal (sizes in mm) results and those on filament growth may not be meaningful. Filament growth requires a small crystal size (R) (below 0.5 μm in size) and consequently a large diffusion time constant, D/R^2, where D is the diffusivity of carbon in metal. (The reciprocal of the time constant is an indication of the time required for diffusion through the metal.) A small time constant, as in large crystals, results in an increased diffusion resistance

relative to the surface decomposition rate, and consequently causes carbon buildup on the surface. This is similar to carbon "encapsulation" on small particles which terminates the filament growth process.

Driving Force and Mechanism for Filament Growth

Continual filament growth requires sustained diffusion of carbon. The hypothesis of a concentration-driven process was proposed (37) based on the work of Wada et al. (38) and that of Lander et al. (39). It was deduced, from the latter work, that supersaturation of carbon in nickel could occur at the gas/nickel interface when the activity of carbon in the gas phase exceeded unity (37). In the work reported in Refs. (38) and (39), H_2/CH_4 mixtures were used to carburize Ni. The activity of carbon in the gas phase, a_c, is given by

$$a_c = K \frac{P_{CH_4}}{P_{H_2}^2} \qquad (1)$$

for the equilibrium $CH_4 \rightleftarrows C + 2H_2$, where K is the equilibrium constant and P is partial pressure. Wada et al. kept $a_c \leq 1$ in their experiments and did observe, in one experiment, that graphite precipitated on Ni surface when a H_2/CH_4 mixture corresponding to $a_c = 1.03$ was used (38). They further showed a sizable scatter among the published data on the solubility of graphite in nickel. Comparing with the more recent data by Eizenberg and Blakely (15), the published solubility data for C/Ni follow the order Eizenberg/Blakely = Dunn et al. (40) > Lander et al. > Wada et al. The original hypothesis of a concentration-driven mechanism was based on the assumption that the difference between the data of Lander et al. and those of Wada et al. was due to supersaturation (37), because Lander et al. used a 25/75 CH_4/H_2 mixture where $a_c > 1$. However, the data reported by Eizenberg and Blakely and by Dunn et al. were both equilibrium values with no supersaturation, and their values

were all higher than those of Wada *et al.* Moreover, carbon filament growth seems to occur on all transition metals whereas supersaturation does not. Thus, the basis for the hypothesis of a concentration-driven mechanism remains to be proven.

The alternative hypothesis is the temperature-driven mechanism originally proposed by Baker *et al.* (*41*). Central to the Baker hypothesis is the exothermic heat of decomposition at the gas/metal interface. The precipitation of graphite at the "rear" face is endothermic (40.5 kJ/mol), thus providing a heat sink and sustaining the exothermic decomposition and carbon dissolution at the opposite face (*41*). Experiments with two-dimensional thin films with one side insulated from the hydrocarbon gases showed that carbon diffusion occurred only for exothermic decompositions, and not for endothermic decompositions (*42*). However, filaments have been observed on metal powders from endothermic decompositions, e.g., decompositions of CH_4, C_4H_{10}, C_6H_{14}, and butenes. Thus, major differences exist between carbon deposition on fine particles and that on two-dimensional films. Heat transfer from the surroundings to the metal is primarily by radiation at the reaction temperatures. For an equal area of gas/metal interface, the radiation received by a particle is much greater than that by a thin film. Consequently, for fine particles, exothermality is not a necessary condition for sustained carbon diffusion, becuase the large amount of radiation can compensate for the endothermic heat of reaction.

From the above discussion and the results obtained in this work, a different temperature-driven mechanism for filament growth seems reasonable, as described below. A temperature gradient across the particle may be maintained by the endothermic graphite precipitation at the graphite/metal interface and the exothermic carbon dissolution at the gas/metal interface. For endothermic decomposition, the heat may be supplied by the radiation from the surroundings to the gas/metal interace. Graphite precipitation at the cooler graphite/metal interface creates a sink for carbon diffusion. The onset of the precipitation is, however, not understood. From the results of Blakely *et al.* (*14–16*), phase segregation (to form a monolayer of carbon) occurs on many faces when the carbon concentration in the metal is well below its saturation, e.g., at about one-half of the saturation solubility for C/Ni. Further decomposition/dissolution brings the concentration in the particle to saturation, which represents a highly unstable state. A slight perturbation would initiate the graphite precipitation process, which continues until all gas/metal interfaces are encapsulated. The initiation and encapsulation processes are poorly understood at present.

CONCLUSION

A study is made on carbon filament growth on fine particles (<0.5 μm in size) of α-Fe, Co, and Ni from CH_4 at 700°C. The metal particles are faceted single crystals after filament growth. TEM/SAD results show that the (100) and (110) faces are among the gas/metal interfaces and the (111) and (311) faces are among the graphite/metal interfaces. EHMO calculations indicate that the Ni(111) and (311) faces provide the strongest epitaxial covalent bonds with the basal plane of graphite, and the Ni(100) and (110) faces are most active in decomposition to form carbon. On the basis of these results and the literature information on carbon segregation and precipitation as well as metal surface reconstruction upon carbon segregation, the following mechanistic steps are suggested for carbon filament growth. Carbon is first formed and dissolved in metal, followed by graphite/metal segregation and metal reconstruction/faceting. This is the period observed as the incubation period. The ensuing step is a steady-state filament growth period involving decomposition of hydrocarbon on the gas/metal interfaces and graphite precipitation on the graphite/metal

interfaces. This step continues until the gas/metal interfaces are encapsulated by carbon. The basis for the concentration-driven mechanism for steady-state filament growth as suggested in the literature is inadequate. A temperature-driven mechanism without resorting to surface reaction exothermality is proposed. These two driving forces are not mutually exclusive and may both contribute to filament growth.

ACKNOWLEDGMENTS

REFERENCES

1. Trimm, D. L., *Catal. Rev. Sci. Eng.* **16,** 155 (1977).
2. Baker, R. T. K., and Harris, P. S., *in* "Chemistry and Physics of Carbon" (P. L. Walker, Jr. and P. A. Thrower, Eds.), Vol. 14, p. 83. Dekker, New York, 1978
3. Bartholomew, C. H., *Catal. Rev. Sci. Eng.* **24,** 67 (1982).
4. Wolf, E. E., and Alfani, P., *Catal. Rev. Sci. Eng.* **24,** 329 (1982).
5. Baker, R. T. K., Yates, D. J. C., and Dumesic, J. A., *in* "Coke Formation on Metal Surfaces" (L. F. Albright and R. T. K. Baker, Eds.), p. 1. Amer. Chem. Soc., Washington, DC, 1982.
6. Baird, T., Fryer, J. R., and Grant, B., *Nature (London)* **233,** 329 (1971).
7. Audier, M., Oberlin, A., and Coulson, M., *J. Cryst. Growth* **55,** 549 (1981).
8. Audier, M., Coulson, M., and Oberlin, A., *Carbon* **19,** 217 (1981).
9. Boellaard, E., De Bokx, P. K., Kock, A. J. H. M., and Geus, J. W., *J. Catal.* **96,** 481 (1985).
10. Sacco, A., Thacker, P., Chang, T. N., and Chiang, A. T. S., *J. Catal.* **85,** 224 (1984).
11. De Bokx, P.K, Kock, A. J. H. M., Boellaard, E., Klop, W., and Geus, J. W., *J. Catal.* **96,** 454, 468, 481 (1985).
12. Tibbetts, G. G., Devour, M. G., and Rodda, E. J., *Carbon* **25,** 367 (1987).
13. Alstrup, I., *J. Catal.* **109,** 241 (1988).
14. Shelton, J. C., Patil, H. R., and Blakely, J. M., *Surf. Sci.* **43,** 493 (1974).
15. Eizenberg, M., and Blakely, J. M., *Surf. Sci.* **82,** 288 (1979); *J. Chem. Phys.* **71,** 3467 (1979).
16. Hamilton, J. C., and Blakely, J. M., *Surf. Sci.* **91,** 199 (1980).
17. Hoffman, R., *J. Chem. Phys.* **39,** 1397 (1963).
18. Bartmess, J. E., and Thomas, D., Quantum Chemistry Program Exchange, QCPE Program No. QCMP 011, Indiana University, Department of Chemistry, 1988.
19. Baetzold, R. C., *J. Catal.* **29,** 129 (1973).
20. Baetzold, R. C., *in* "Advances in Catalysis" (D. D. Eley, H. Pines, and P. B. Weisz, Eds.), Vol. 25, p. 1. Academic Press, New York, 1976.
21. Zhidomirov, C. M., and Kazansky, V. B., *in* "Advances in Catalysis" (D. D. Eley, H. Pines, and P. B. Weisz, Eds.), Vol. 34, p. 131. Academic Press, New York, 1986.
22. Kusuma, T. S., and Companion, A. L., *Surf. Sci.* **195,** 59 (1988).
23. Casalone, G., Merati, F., and Tantardini, G. F., *Chem. Phys. Lett.* **137,** 234 (1987).
24. Mitchell, G. F., and Welch, A. J., *J. Chem. Soc. Dalton Trans.* **5,** 1017 (1987).
25. King, R. B., *J. Comp. Chem.* **8,** 341 (1987).
26. Mulliken, R. S., *J. Chem. Phys.* **23,** 1833 (1955).
27. Robertson, J. C., and Wilmsen, C. W., *J. Vac. Sci. Technol.* **9,** 901 (1972).
28. Hedberg, L., Iijima, T., and Hedberg, K., *J. Chem. Phys.* **70,** 3224 (1979).
29. Blyholder, G., *J. Phys. Chem.* **68,** 2772 (1964).
30. Andrews, K. W., Dyson, D. J., and Keown, S. R., "Interpretation of Electron Diffraction Patterns." Plenum, New York, 1971.
31. Panas, I., Schule, J., Brandemark, U., Siegbahn, P., and Wahlgren, U., *J. Phys. Chem.* **92,** 3079 (1988).
32. Kehrer, V. J., and Leidheiser, H., Jr., *J. Phys. Chem.* **58,** 550 (1954).
33. LaCava, A. I., Fernandez-Rane, E. D., Issacs, L., and Caraballo, M., *in* "Coke Formation on Metal Surfaces" (L. F. Albright and R. T. K. Baker, Eds.). American Chemical Soc., Washington, DC, 1982.
34. Schouten, F. C., Gijzeman, O. L. J., and Bootsma, G. A., *Surf. Sci.* **87,** 1 (1979).
35. Presland, A. E. B., Roscoe, C., and Walker, P. L., Jr., "Third Conf. Indust. Carbon and Graphite," p. 116. Soc. Chem. Ind., London, 1970.
36. Van Hove, M. A., Koestner, R. J., Stair, P. C., Biberian, J. P., Kesmodel, L. L., Bartos, I., and Somorjai, G. A., *Surf. Sci.* **103,** 189 (1981).
37. Rostrup-Nielsen, J., and Trimm, D.L., *J. Catal.* **48,** 155 (1977).
38. Wada, T., Wada, H., Elliott, J. F., and Chipman, J., *Metal. Trans.* **2,** 2199 (1971).
39. Lander, J. J., Kern, H. E., and Beach, A. L., *J. Appl. Phys.* **3,** 1305 (1952).
40. Dunn, W. W., McLellan, R. B., and Oates, W. A., *Trans. TMS-AIME* **242,** 2129 (1968).
41. Baker, R. T. K., Barber, M. A., Harris, P. S., Feates, F. S., and Waite, R. J., *J. Catal.* **26,** 51 (1972).
42. Yang, R. T., and Yang, K. L. *J. Catal.* **90,** 194 (1984); **93,** 192 (1985).